

Scaled Particle Theory for Hard Sphere Pairs. II. Numerical Analysis

Swaroop Chatterjee and Pablo G. Debenedetti

Department of Chemical Engineering,

Princeton University, Princeton, NJ 08544, USA

Frank H. Stillinger

Department of Chemistry, Princeton University, Princeton, NJ 08544, USA

(Dated: February 6, 2008)

Abstract

We use the extension of scaled particle theory (ESPT) presented in the accompanying paper [Stillinger et al. J. Chem. Phys. xxx, xxx (2007)] to calculate numerically pair correlation function of the hard sphere fluid over the density range $0 \leq \rho\sigma^3 \leq 0.96$. Comparison with computer simulation results reveals that the new theory is able to capture accurately the fluid's structure across the entire density range examined. The pressure predicted via the virial route is systematically lower than simulation results, while that obtained using the compressibility route is lower than simulation predictions for $\rho\sigma^3 \leq 0.67$ and higher than simulation predictions for $\rho\sigma^3 \geq 0.67$. Numerical predictions are also presented for the surface tension and Tolman length of the hard sphere fluid.

I. INTRODUCTION

During roughly the last half century, the statistical mechanics of many-body systems has incorporated and has benefited from various forms of computer simulation. Indeed, with the remarkable advances in computer power that have occurred during that period, simulation has grown in the depth and breadth of its contributions to a point of near dominance over more analytical approaches. The hard sphere model provides a clear example, where its rich repertoire of both equilibrium and non-equilibrium phenomena are now better appreciated and understood as a result of a wide range of simulation activities^{1,2,3,4,5}.

Nevertheless, continuing to pursue the more analytical aspects of many-body statistical mechanics remains a valuable complementary mission. This and the immediately preceding companion paper⁶ (hereafter referred to as "I"), fall into this more analytical category. The objective has been to deepen understanding of the equilibrium properties of the classical hard sphere system. The underlying strategy involves an extension (ESPT) of the "scaled particle theory" (SPT) originally presented by Reiss, Frisch, and Lebowitz⁷. The mathematical strategy of our approach has been described in "I". The present paper "II" provides details of a numerical investigation based on the mathematical formalism developed in "I". One of our principal objectives is numerical prediction of the hard sphere pair correlation function $g(r, \rho)$ over a substantial range in density ρ .

The following Section II describes the coupled equations that must be self-consistently solved. At the center of this procedure is a non-linear integral equation for $g(r, \rho)$. Successful solution of this equation at high density demands use of somewhat sophisticated techniques that are explained in Section II. Section III presents results not only for the basic quantity $g(r, \rho)$, but also for the pressure and surface free-energy properties of the hard sphere system. This investigation has inevitably raised some important questions, particularly about what might be the most profitable directions for future extensions of the approach. These questions and our conclusions based on the results obtained thus far form the subjects for Section IV.

II. NUMERICAL PROCEDURE

The goal of our numerical calculations is to obtain the hard sphere pair correlation function $g(r, \rho)$. In “I”, we introduced the overall general strategy behind this calculation. Here, we outline the solution procedure in greater detail. The computation can be divided into two major parts. The first involves the calculation of the isothermal reversible work $W(\lambda, \rho)$ required to create a single spherical cavity in a hard sphere fluid, where λ is the cavity radius, and the second involves the calculation of the double or bi-spherical isothermal and reversible cavity formation work $W_2(r, \lambda, \rho)$, where r is the separation between the two cavity centers. By calculating the work done in these two cases, the pair correlation function can be obtained using the following relation ($\beta = 1/k_B T$):

$$g(r, \rho) = \exp[-\beta W_2(r, 1, \rho) + 2\beta W(1, \rho)] \quad (1)$$

To use the above relation, we note that the cavity work terms $W(\lambda, \rho)$ and $W_2(r, \lambda, \rho)$ must be evaluated at $\lambda = \sigma$, the hard sphere diameter (i.e., $\lambda = 1$, using σ as the natural scale for distance). Using the extended scaled particle theory (ESPT) of “I”, the single cavity work is described by the following set of equations for different ranges of λ :

$$\beta W(\lambda, \rho) = -\ln \left(1 - 4\pi\rho\lambda^3/3 \right), \quad \left(0 \leq \lambda \leq \frac{1}{2} \right) \quad (2)$$

$$= -\ln \left(1 - 4\pi\rho\lambda^3/3 + 2\pi^2\rho^2 \int_1^{2\lambda} dr \left[4\lambda^3r^2/3 - \lambda^2r^3 + r^5/12 \right] g(r, \rho) \right), \quad \left(\frac{1}{2} \leq \lambda \leq 3^{-1/2} \right) \quad (3)$$

$$= J(\rho)\lambda^3 + K(\rho)\lambda^2 + L(\rho)\lambda + M(\rho) + N(\rho)/\lambda, \quad \left(\frac{1}{3^{1/2}} \leq \lambda \right) \quad (4)$$

Therefore, the calculation of $W(\lambda = 1, \rho)$ requires finding the coefficients $J \dots N$ such that $W(\lambda, \rho)$ is a smooth function of λ . Among these, the coefficient J is related to the pressure P , K to the surface tension γ and L to its curvature dependence. The fitting of these coefficients is performed at $\lambda = 3^{-1/2}$. In other words, we use the expressions given in the equations 3 and 4 to calculate values of the coefficients that ensure a smooth transition across $\lambda = 3^{-1/2}$. This is accomplished by equating the work function value, along with its first and second λ -derivatives, in the two regions (equations 3 and 4) providing constraints on three of the five coefficients. The other two necessary conditions are obtained by evaluating

the pressure P , and hence $J(\rho)$ from the pair correlation function

$$J(\rho) = \frac{4\pi}{3}\beta P = \frac{4\pi\rho}{3} + \frac{8\pi^2\rho^2}{9}g(1, \rho) \quad (5)$$

and the following condition arising from the density of particle centers $\rho g(r, \rho)$ at the surface of the $\lambda = 1$ cavity

$$\beta W'(r, \lambda = 1) = 4\pi\rho g(1, \rho) \quad (6)$$

We note here that in this $W(\lambda, \rho)$ calculation, $g(r, \rho)$ is required as input to evaluate the necessary conditions. We will further address this issue later on in this section.

Having obtained $W(\lambda = 1, \rho)$, we turn our attention to the bi-spherical cavity work $W_2(r, \lambda, \rho)$. This calculation follows along similar lines as in the single cavity case. In “I”, we developed expressions for the $W_2(r, \lambda, \rho)$ for two regimes: one where the range of cavity sizes (λ) limits the maximum possible number of clusters of spheres of unit diameter that can be found inside the bi-spherical cavity to 2, and the other where the maximum occupancy is greater than 2. We display them here in a different form.

$$\begin{aligned} \beta W_2(r, \lambda, \rho) = & -\ln \left\{ 1 - \rho V(r, \lambda) + \frac{2\pi^2\rho^2}{r} \int_{r-2\lambda}^r dr_1 \right. \\ & \left(\frac{8}{15}\lambda^5 - \frac{2}{3}\lambda^3(r-r_1)^2 + \frac{1}{3}\lambda^2(r-r_1)^3 - \frac{1}{60}(r-r_1)^5 \right) r_1 g(r_1) + \frac{2\pi^2\rho^2}{r} \int_r^{r+2\lambda} dr_2 \right. \\ & \left. \left(\frac{8}{15}\lambda^5 - \frac{2}{3}\lambda^3(r-r_2)^2 - \frac{1}{3}\lambda^2(r-r_2)^3 + \frac{1}{60}(r-r_2)^5 \right) r_2 g(r_2) \right\}, \text{ for } n = 2 \end{aligned} \quad (7)$$

$$\beta W_2(r, \lambda, \rho) = \frac{3J(\rho)}{4\pi}V(r, \lambda) + \frac{K(\rho)}{4\pi}A(r, \lambda) + X(\rho, s)\lambda + Y(\rho, s) + \frac{Z(\rho, s)}{\lambda}, \text{ for } n \geq 2 \quad (8)$$

where $V(r, \lambda)$ and $A(r, \lambda)$ are the volume and surface area of the double cavity, and s is a transformation variable defined as $s = r - 2\lambda$. Physically, s describes the distance between the nearest points on the surface of the two spherical cavities, when they are disconnected, and the corresponding distance between the interpenetrating surfaces, when they overlap. In the former case, s is positive and it is negative in the latter case. Using this variable allows us to circumvent singularities arising due to the disconnection of the two cavities of size λ at $r = 2\lambda$.

The boundary between the two regimes, as discussed in “I”, for $r \geq (3^{1/2} - 1)/2$ is at $\lambda = 1/2$, and for $0 \leq r < (3^{1/2} - 1)/2$ is given by $\lambda = (1/2)(3^{1/2} - r) + (1/8)(3^{1/2} - r)^{-1}$, where we have expressed distances in units of σ . We assume that equation 8 holds for all r , provided $\lambda > 1/2$. Furthermore, coefficients $J(\rho)$ and $K(\rho)$ are the same as those obtained

in the single cavity $W(\lambda, \rho)$ calculation. Therefore, there are three coefficients that need to be determined, namely $X(\rho, s)$, $Y(\rho, s)$ and $Z(\rho, s)$. These are determined by equating the value of the work function W_2 , and its first and second derivatives with respect to λ at $\lambda = 1/2$.

Along with the transformation variable s , another variable $t = 2\lambda - 1$, a rescaled and shifted cavity size, is also used. In these variables, the fitting described above is done for each s value at $t = 0$. The pair correlation calculation in equation 1 therefore requires that the coefficients X , Y and Z be determined for various values of the intercavity distance s at $t = 1$. The range of s in this calculation is $-1 \leq s < \infty$, which corresponds to $1 \leq r < \infty$.

Once all eight coefficients $J(\rho)$, $K(\rho)$, $L(\rho)$, $M(\rho)$, $N(\rho)$, $X(\rho, s)$, $Y(\rho, s)$, and $Z(\rho, s)$ are computed, the calculation of $g(r, \rho)$ follows from equation 1 by setting $\lambda = 1$ in the single cavity work $W(\lambda, \rho)$ calculation and $t = 1$ in the double cavity $W_2(s, t, \rho)$ calculation. However, as noted earlier in this section, both work calculations require $g(r, \rho)$ as input (see equations 3 and 7). To accomplish this pair correlation function calculation, a numerical solution technique is employed by using an estimate of $g(r, \rho)$ as input, and then iteratively correcting it after calculating $g(r, \rho)$ using the procedure discussed above. An arbitrarily small tolerance is chosen to determine whether the calculation has converged by comparing the calculated and input $g(r, \rho)$ functions.

An appropriate numerical method to correct the input $g(r, \rho)$ using the calculated values was determined after some trials on our part. The first attempted technique simply used a linear combination of the n^{th} step input and calculated values in some arbitrary proportion to obtain the $(n + 1)^{th}$ step input $g(r, \rho)$. In other words,

$$g_{n+1}^{input}(r, \rho) = x \times g_n^{input}(r, \rho) + (1 - x) \times g_n^{calculated}(r, \rho) \quad (9)$$

where x defines the proportion of calculated and input value in the corrected input $g(r, \rho)$ for the next stage. This method is only effective at low densities ($\rho < 0.4$; here and in the remainder of the paper, dimensionless densities are obtained by scaling with σ , the hard sphere diameter), regardless of the value assigned to x . The reason for this might be the high degree of non-linearity in the problem, which makes it difficult to achieve convergence using such a crude technique if the initial input $g(r, \rho)$ is not an accurate enough estimate of the actual function. In this connection, we used, as two alternative input $g(r, \rho)$'s, a polynomial extrapolation of the converged pair correlation functions obtained for densities

lower than the one being computed, or the converged pair correlation function of a lower density case. These changes are able to improve the overall speed and convergence of the calculation. However, beyond a density $\rho \cong 0.6$, even these methods are unable to ensure convergence of the calculation.

Satisfactory behavior in both convergence and speed was eventually obtained by using a generalized minimum residual method (GMRES) to solve the system of equations. The conventional GMRES method was developed for systems of linear equations⁸. It can be shown that for linear equations, the solution can be approximated by the n^{th} iterate of the vector in a Krylov subspace (defined below) which minimizes the residual. Mathematically, for a system of equations of the form $Ax = b$, where x is the variable to be solved, the n^{th} Krylov subspace is given by

$$K_n = \text{span}\{b, Ab, A^2b, \dots, A^{n-1}b\} \quad (10)$$

where $\text{span}\{z_1, z_2, \dots\}$ refers to the set of linearly dependent vectors which can be constructed from a vector set z_1, z_2, \dots . The solution using the GMRES method is a vector in this subspace $x_n \in K_n$ such that the norm of residual $Ax_n - b$ is minimized as part of a least-squares problem. In order to solve this problem, we need to find the orthonormal basis vectors of K_n . The component vectors in the above equation ($b, Ab, \dots, A^{n-1}b$), being linearly dependent, are therefore not suitable to form this basis vector set. Instead, the Arnoldi process⁹ is used to construct the necessary orthonormal basis vectors v_1, \dots, v_n of K_n . This process also produces an upper Hessenberg matrix H_n of dimensions $n + 1$ by n such that

$$Av_n = v_{n+1}H_n \quad (11)$$

The orthogonality of the basis vectors leads to a simplification in the least-squares problem, or in other words the objective function is altered as

$$\min_{x_n \in K_n} \|Ax_n - b\| \equiv \min_{y_n \in \mathbb{R}^n} \|H_n y_n - e_1\| \quad (12)$$

where

$$y_n = x_n/v_n \quad (13)$$

and $e_1 = (1, 0, 0, \dots, 0)$ is the first standard basis vector of \mathbb{R}^n . At each step in the solution procedure, GMRES solves for y_n and then uses equation 13 to find x_n . This process is

repeated with increasing value of n until the residual $\| H_n y_n - e_1 \|$ is within an assigned tolerance value.

This general approach, although originally developed for systems of linear equations, has been extended to handle nonlinear equations¹⁰. The main difference lies in the objective function. In solving a system of nonlinear equations $F(x) = 0$, the least squares problem at each step in the calculation is formulated as $\min_{s_n \in K_n} \| F(x_n) + F'(x_n)s_n \|$ where s_n is related to x_n by the equation

$$s_n = s_0 + x_n \quad (14)$$

where s_0 is a chosen parameter. The GMRES method can be shown to find a solution to a linear system of equations in at most n iterations⁸. For the nonlinear system of equations, however, no such guarantees can be made. As a result, a maximum number of iterations (n_{max}) is set. If the residual is not within the set tolerance value after n_{max} iterations, the calculation is restarted such that $s_0 = s_{n_{max}}$. A maximum number of restarts is also used as input to the method so that the calculation can be terminated in the event that convergence is not achieved. The maximum distance r_{max} was set at $r = 9$ for these $g(r, \rho)$ calculations. The computation interval $1 \leq r \leq r_{max}$ was divided into 2000 discrete intervals, and Simpson's rule was used in all integrations.

The major thrust of this paper has been to calculate the pair correlation function $g(r, \rho)$ for a hard sphere fluid based on the extended scaled particle theory (ESPT) of "I". Using the methods discussed in this and the previous section, $g(r, \rho)$ has been computed for different densities. As an initial estimate for each $g(r, \rho)$ calculation, the converged $g(r, \rho)$ for a lower density case was used. A tolerance limit of 10^{-7} was set for each calculation to determine whether the residual was low enough.

III. RESULTS

The solution scheme described in the previous section was used to obtain the equilibrium pair correlation function $g(r, \rho)$ for the hard sphere fluid. We compare the $g(r, \rho)$ obtained for different densities in Figs. 1, 2 and 3. The same figures also compare the calculated values of $g(r, \rho)$ with those obtained from molecular dynamics simulations¹¹. In general, the ESPT prediction for $g(r, \rho)$ is in very good agreement with molecular dynamics calculations, indicating the success of the theory in capturing fluid structure and its density dependence.

However, for $\rho \geq 0.4$, the theory underpredicts $g(1, \rho)$, as will be discussed in connection with equation of state predictions.

The computation time required for each successive calculation to converge increases with density. In this work, we have been able to continue the pair correlation calculations to densities that are in the metastable region of the accepted hard sphere phase diagram. The generally accepted freezing density for the hard sphere fluid is $\rho_{freezing} = 0.943$ ⁴. In Fig. 3(c), the pair correlation function based on the ESPT for a density $\rho = 0.96$ is shown. The second peak appears to be almost triangular in shape instead of the smooth peak observed at lower densities. Note that the development of this near-triangular peak shape is also evident in the molecular dynamics simulation results. Calculations of the pair correlation function for $\rho > 0.96$ using the above discussed numerical scheme do not converge. Further refinement of the numerical approach is under investigation.

The contact value $g(\sigma, \rho)$ can be used to calculate the pressure of the fluid P using the virial theorem,

$$\beta P = \rho + (2/3)\pi\rho^2\sigma^3g(\sigma, \rho) \quad (15)$$

In Fig 4, the pressure is plotted against density for the ESPT along with predictions from other equations of state (EOS's) for the hard sphere fluid. The pressure prediction from the ESPT of “T” corresponds closely to molecular simulation results¹² at low densities. However at higher densities, there is significant deviation between the two. In fact, we find that the ESPT pressure is very close to the corresponding quantity computed via the Percus-Yevick closure¹³ (pressure equation). This, in itself, is an interesting result in light of the fact¹⁴ that the original SPT of Reiss et al.⁷ produces the same EOS as the Percus-Yevick closure (compressibility equation)¹³. Both versions of SPT are unable to accurately predict the pressure at higher densities. The original SPT over-estimates the pressure, while the ESPT underestimates it.

An alternative calculation can be conducted using the isothermal compressibility equation

$$\beta\left(\frac{\partial\rho}{\partial P}\right)_T = 1 + 4\pi\rho \int [g(r, \rho) - 1]r^2 dr \quad (16)$$

The derivative $(\partial P/\partial\rho)_T$ can then be integrated numerically from the ideal gas limit, [$\beta P = \rho$; $g(r, \rho) = 1$ for $r > 1$, as $\rho \rightarrow 0$]. We use density steps of $\delta\rho = .02$ in this calculation, ensuring that computed dimensionless pressure values, $P\sigma^3/(k_B T)$, are accurate within 10^{-2} .

A cut-off distance in r is selected such that contributions to the integral in equation 16 are considered only when $|g(r, \rho) - 1|$ at any peak of $g(r, \rho)$ is greater than 2×10^{-3} . The pressure obtained by this route is shown in Fig. 5. In the figure, we compare the EOS predictions from equations 15 and 16 with the corresponding original SPT prediction⁷. At high densities, the ESPT calculation via the compressibility equation closely matches the original SPT, or equivalently¹⁴, the Percus-Yevick compressibility calculation. However, at low density, there is significant difference between the two, with the ESPT compressibility calculation yielding lower pressures. The same figure with the accompanying inset also displays EOS values as obtained from molecular simulation results. The EOS prediction from ESPT through the compressibility route underpredicts the pressure at lower densities ($\rho \leq 0.67$) and overpredicts this quantity at higher densities ($\rho \geq 0.67$), when compared to simulation results.

The surface tension of the hard sphere fluid can be estimated from the parameter K in the asymptotic form of the cavity formation work $\beta W(\lambda, \rho)$ in equation 4

$$\beta\gamma = \frac{K}{4\pi} \quad (17)$$

where γ is the surface tension. A comparison of γ from the ESPT with that of the original SPT is shown in Fig. 6. The original SPT has been shown to predict, with reasonable accuracy, the surface tension of the hard sphere fluid, when compared to simulation results¹⁵. Both theories predict negative surface tension for the hard sphere fluid with γ increasing in magnitude with increasing density. Similar values of γ are predicted by both theories at low and high densities. However, for intermediate densities, the ESPT predicts a smaller magnitude for the surface tension than the original SPT. Comparison with simulation results^{16,17,18} is shown in Fig. 7. Here, the pressure prediction for the different theories and simulations is plotted on the abscissa. We observe that the ESPT is able to provide a more accurate prediction of the surface tension at low density and pressure. However as the density increases, the original SPT is able to more accurately capture the dependence of surface tension on pressure. Equation 16 provides an alternate route for the calculation of the EOS using the ESPT. As shown in Fig. 8, use of the compressibility route enables the ESPT to provide an improved representation of simulation results for the variation of surface tension with pressure than the original SPT.

The Tolman length δ is a measure of the dependence of surface tension on curvature. It

can be estimated from parameter L in the asymptotic equation 4 from the following relation

$$\delta = -\frac{Lk_B T}{8\pi\gamma} \quad (18)$$

For a hard sphere fluid $\delta > 0$. The predicted variation of δ with density is shown in Fig. 9. The Tolman length increases monotonically upon compression. Comparing these values with those from the original SPT, we find that ESPT predicts a more pronounced dependence of the surface tension on curvature.

IV. CONCLUSIONS

A new scaled particle theory of hard sphere pairs⁶ has been used to calculate the pair correlation function $g(r, \rho)$ of the hard sphere fluid over a wide range of densities, covering the generally accepted stable and slightly metastable fluid states. Comparison with results from molecular dynamics simulations¹¹ shows that the extended scaled particle theory (ESPT) is able to accurately describe the fluid's structure, but it underestimates the $g(r, \rho)$ contact value when $\rho > 0.4$. The theory is able to accurately reproduce the shape of the peak corresponding to second neighbor shell at $r \cong 2$ which becomes sharper as the density of the hard sphere fluid increases, in agreement with simulation results.

The ESPT has been used to compute the equation of state of the hard sphere fluid by using the virial theorem. The calculated EOS values correspond closely at lower densities with those obtained from molecular simulations¹². However, there are significant differences between the two at higher densities. We find that ESPT consistently underpredicts EOS values from molecular simulation. This can be contrasted against the overprediction of the EOS by the original SPT. Comparing the predictions of ESPT with those from other theories, we find that the calculated EOS values closely match those computed using the Percus-Yevick approximation (pressure equation). We have also calculated the hard sphere equation of state using ESPT with the compressibility equation. The resulting prediction is close to the equation of state obtained using the Percus-Yevick closure and the compressibility equation, especially at high densities.

The surface tension and Tolman length have also been calculated. As expected, ESPT predicts a negative surface tension for the hard sphere fluid. ESPT is able to more closely capture the pressure dependence of the surface tension at moderate pressures than the

original SPT⁷. However, at higher pressures, the original SPT provides better prediction. As discussed above, employing the compressibility route improves the EOS prediction of ESPT, leading to a closer correspondence with γ vs. P surface tension predictions from molecular simulation. ESPT predicts a larger Tolman length than the original SPT, or in other words, the new theory predicts a more pronounced effect of curvature on surface tension than the original theory.

Having studied a small portion of the metastable branch of the equation of state, future research directions might include an examination of the high density range of the phase diagram in an attempt to calculate the pair correlation function of both the hard sphere solid and the metastable fluid. Using solid and fluid forms of $g(r, \rho)$ as initial inputs to the calculation is a possible strategy that will be investigated as a means of testing the present theory's ability to predict a freezing transition. Further numerical work is needed to ensure convergence along the high-density metastable branch.

Another avenue of investigation is to extend the current hard sphere theory to study solvation effects. The new theory would include the effect of orientation of and attraction between interacting particles. There have been other attempts at developing such theories in the past^{19,20}. These have been successful in highlighting important phenomena associated with hydrophobic hydration or solvation.

Finally, we point out that additional consistency conditions can be imposed in the iteration scheme described in Section III. The extent to which such additional constraints improve the accuracy of ESPT predictions of thermodynamic quantities such as the pressure and the surface tension deserves further investigation.

ACKNOWLEDGEMENTS

P.G.D. gratefully acknowledges financial support by the U.S. Department of Energy, Division of Chemical Sciences, Geosciences, and Biosciences, Office of Basic Energy Sciences, grant no. DE-FG02-87ER13714. The authors gratefully acknowledge Yannis Kevrekidis and Liang Qiao for their help with the numerical solution of the non-linear integral equation.

¹ M. N. Rosenbluth and A. W. Rosenbluth, J. Chem Phys. **22**, 881 (1954).

² B. J. Alder, S. P. Frankel, and V. A. Lewinson, J. Chem Phys. **23**, 417 (1955).

³ B. J. Alder and T. E. Wainwright, J. Chem Phys. **33**, 1439 (1960).

⁴ W. G. Hoover and F. H. Ree, J. Chem Phys. **49**, 3609 (1968).

⁵ M. D. Rintoul and S. Torquato, J. Chem Phys. **105**, 9528 (1996).

⁶ F. H. Stillinger, P. G. Debenedetti, and S. Chatterjee, J. Chem. Phys. **xxxxx**, **xxxxx** (2007).

⁷ H. Reiss, H. L. Frisch, and J. L. Lebowitz, J. Chem. Phys. **31**, 369 (1959).

⁸ Y. Saad and M. H. Schultz, SIAM J. Sci. Statist. Comput. **7**, 856 (1986).

⁹ C. T. Kelley, *Iterative Methods for Optimization*, vol. 18 of *Frontiers Appl. Math.* (SIAM, Philadelphia, 1999).

¹⁰ S. Bellavia and B. Morini, SIAM J. Sci. Comput. **23**, 940 (2001).

¹¹ S. Labik and A. Malijevsky, Mol. Phys **42**, 739 (1981).

¹² J. Kolafa, S. Labik, and A. Malijevsky, Phys. Chem. Chem. Phys. **6**, 2335 (2004).

¹³ J. Percus and G. Yevick, Phys. Rev. **110**, 1 (1958).

¹⁴ M. S. Wertheim, Phys. Rev. Lett. **10**, 321 (1963).

¹⁵ D. Siderius and D. Corti, Ind. Eng. Chem. Res. **45**, 5489 (2006).

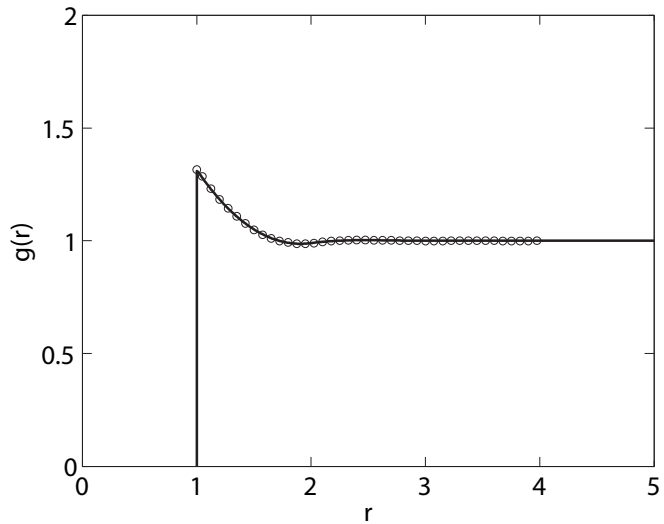
¹⁶ P. Attard and G. A. Moule, Mol. Phys **78**, 943 (1993).

¹⁷ J. R. Henderson and F. van Swol, Mol. Phys **51**, 991 (1984).

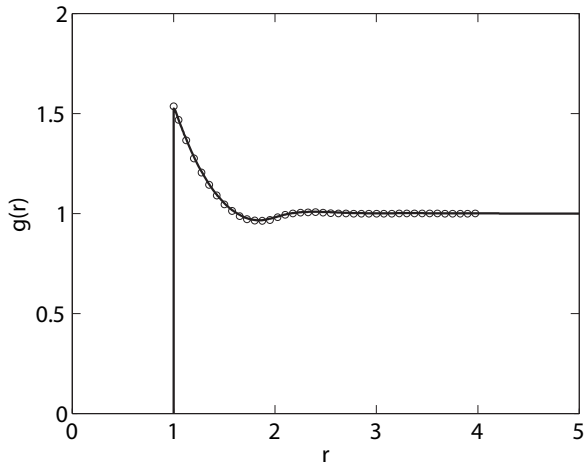
¹⁸ M. Heni and H. Löwen, Phys. Rev. E **60**, 7057 (1999).

¹⁹ H. S. Ashbaugh and L. R. Pratt, Rev. Mod. Phys. **78**, 159 (2006).

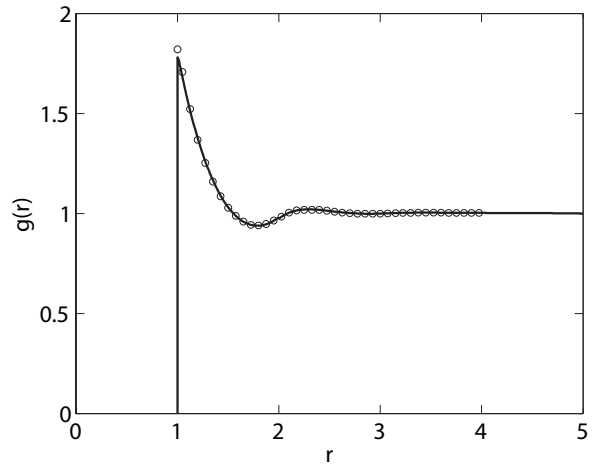
²⁰ F. H. Stillinger, J. Sol. Chem **2**, 141 (1973).



(a)

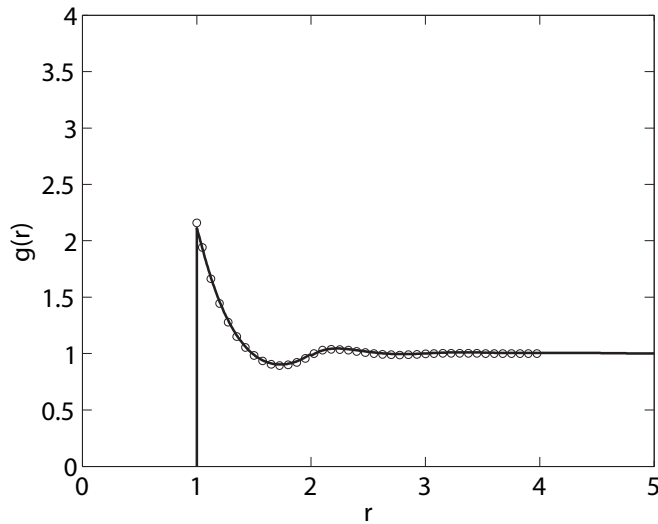


(b)

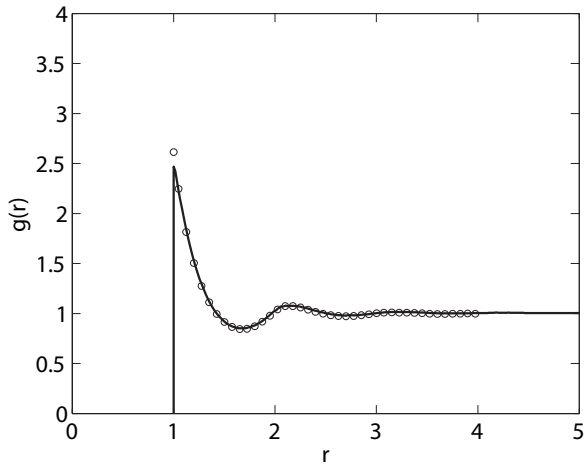


(c)

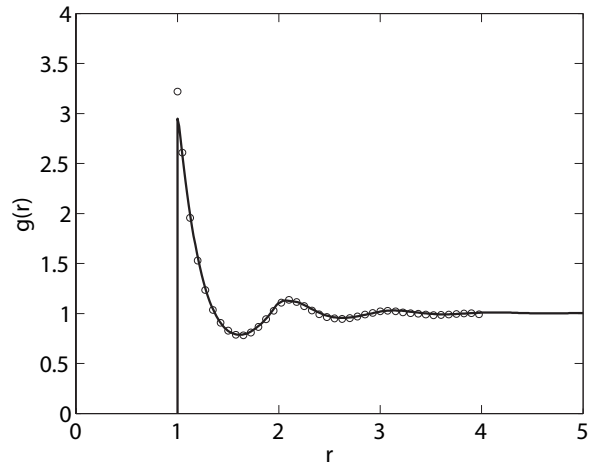
FIG. 1: The pair correlation function obtained using the extended scaled particle theory (ESPT). Here, three densities are shown: (a) $g(r, \rho = 0.2)$, (b) $g(r, \rho = 0.3)$ (c) $g(r, \rho = 0.4)$. The lines are ESPT calculations. The open circles are molecular dynamics simulations¹¹. Distances have been scaled with the hard sphere diameter σ .



(a)

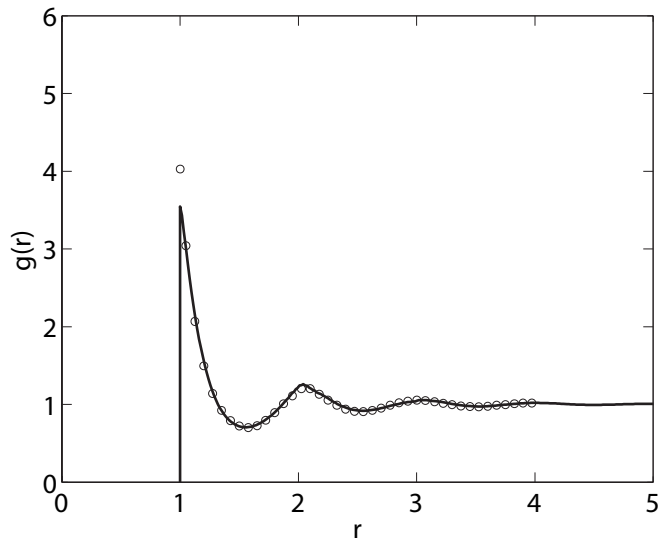


(b)

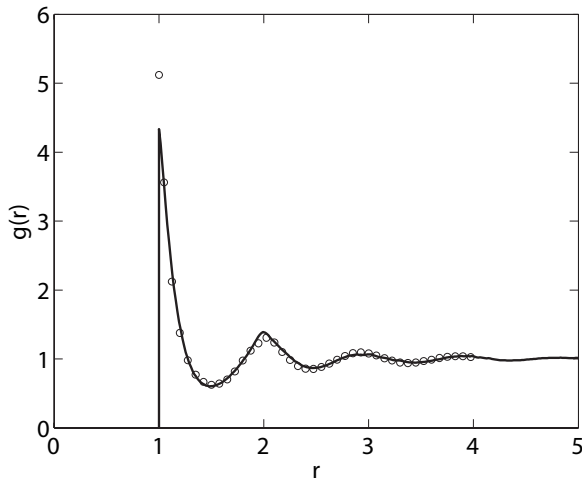


(c)

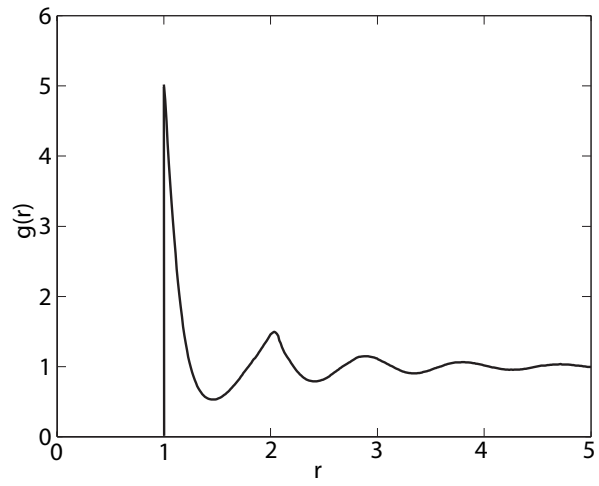
FIG. 2: The pair correlation function obtained using the extended scaled particle theory (ESPT). Here, three densities are shown: (a) $g(r, \rho = 0.5)$, (b) $g(r, \rho = 0.6)$ (c) $g(r, \rho = 0.7)$. The lines are ESPT calculations. The open circles are molecular dynamics simulations¹¹. Distances have been scaled with the hard sphere diameter σ .



(a)



(b)



(c)

FIG. 3: The pair correlation function obtained using the extended scaled particle theory (ESPT). Here, three densities are shown: (a) $g(r, \rho = 0.8)$, (b) $g(r, \rho = 0.9)$ (c) $g(r, \rho = 0.96)$. The lines are ESPT calculations. The open circles are molecular dynamics simulations¹¹. Distances have been scaled with the hard sphere diameter σ .

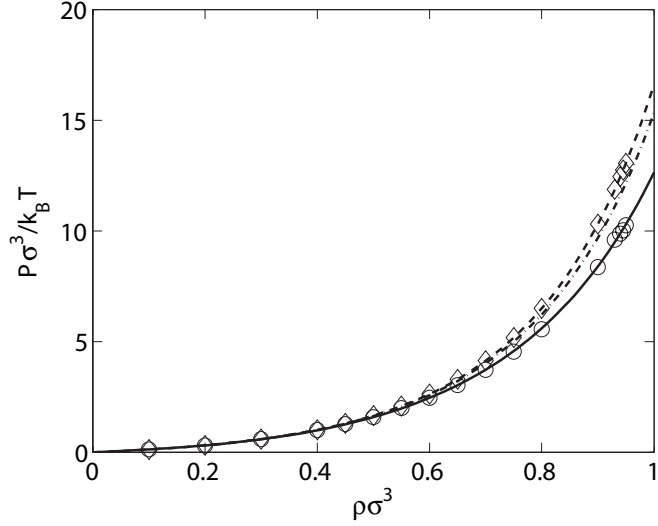


FIG. 4: Equation of state of the hard sphere fluid. We compare predictions from ESPT using equation 15 (\circ), the original SPT of Reiss et al.⁷ (\diamond), the Percus-Yevick¹³ pressure (solid) and compressibility (dashed) calculations, and molecular dynamics simulation results¹² (dot-dashed).

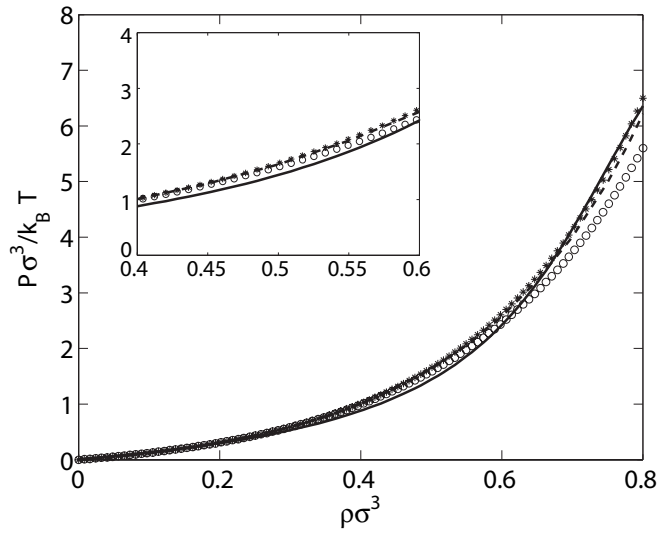


FIG. 5: Equation of state of the hard sphere fluid. We compare predictions from ESPT using the virial (\circ) and the compressibility (solid) routes, the original SPT of Reiss et al.⁷ (*) and molecular dynamics simulation results¹² (dashed). Inset shows details in the density range $0.4 \leq \rho\sigma^3 \leq 0.6$.

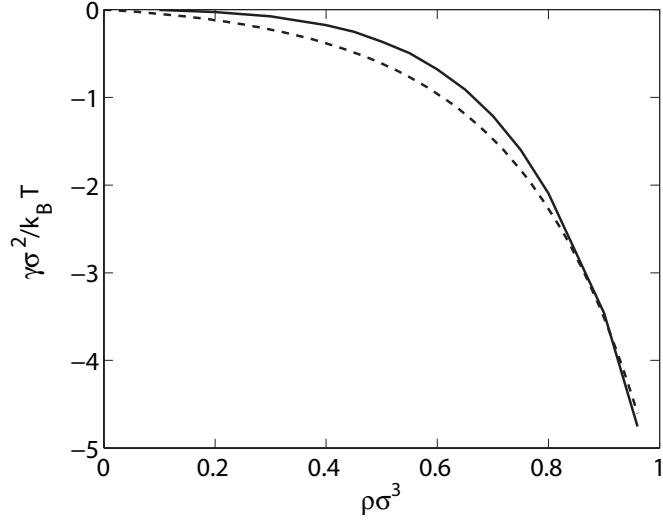


FIG. 6: Surface tension of the hard sphere fluid. The solid line represents the prediction from ESPT; the dotted line, the original SPT of Reiss et al.⁷.

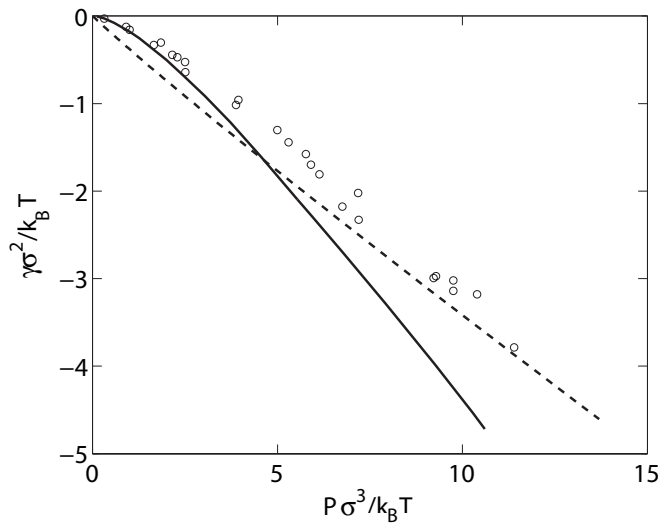


FIG. 7: Surface tension of the hard sphere fluid. The solid line represents the prediction from ESPT using the virial route; the dotted line, the original SPT of Reiss et al.⁷. Open circles (\circ) are simulation results^{16,17,18}.

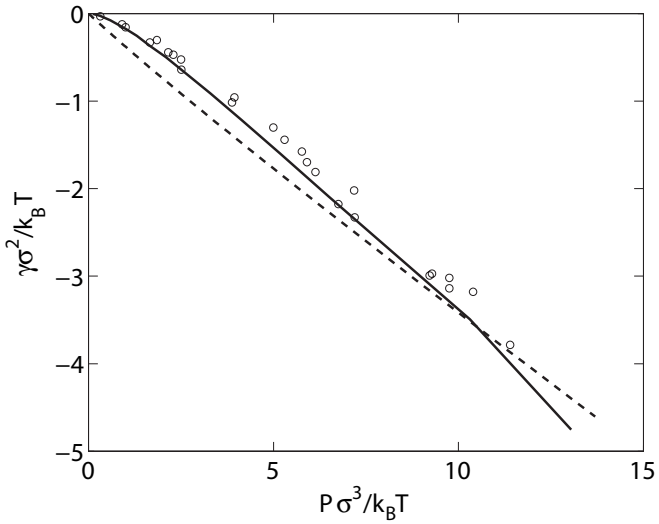


FIG. 8: Surface tension of the hard sphere fluid. The solid line represents the prediction from ESPT using the compressibility route; the dotted line, the original SPT of Reiss et al.⁷. Open circles (\circ) are simulation results^{16,17,18}.

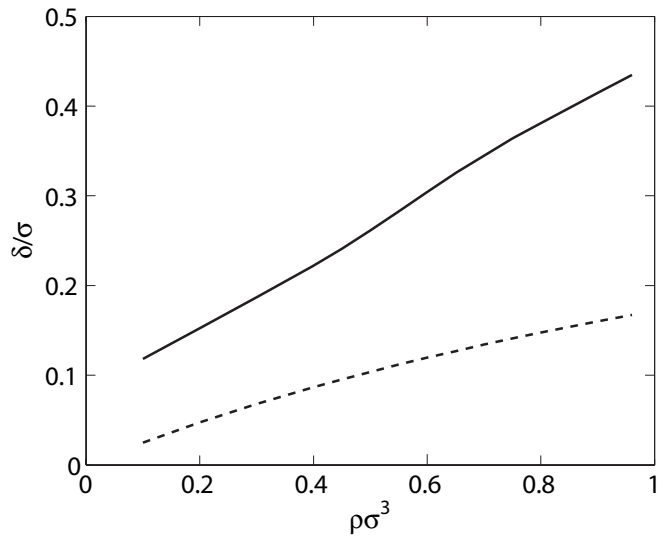


FIG. 9: Tolman length of the hard sphere fluid as predicted by ESPT (solid) and the orginal SPT of Reiss et al.⁷ (dashed).